Line Position and Line Intensity Modelings of H218O up to the First Triad and J = 20

Laurent H. Coudert, Semen Mikhailenko, Alain Campargue, Georg Ch. Mellau

Line position and line intensity modelings of $H_2{}^{18}O$ up to the First Triad and $J = 20$

Laurent H. Coudert,[1, a)] Semen Mikhailenko,[2] Alain Campargue,[3] and Georg Ch. Mellau[4]
[1)] *Université Paris-Saclay, CNRS, Institut des Sciences Moléculaires d'Orsay, 91405 Orsay, France*
[2)] *Laboratory of Theoretical Spectroscopy, V. E. Zuev Institute of Atmospheric Optics, SB, Russian Academy of Science, 1, Academician Zuev Square, 634055 Tomsk, Russia*
[3)] *Univ. Grenoble Alpes, CNRS, LIPhy, Grenoble, France*
[4)] *Physikalisch Chemisches Institut, Justus Liebig Universität Giessen, Giessen, Germany*

(Dated: 6 July 2023)

Line position and line intensity analyses are carried out for the $H_2{}^{18}O$ isotopic species of the water molecule. Both data sets involve the five lowest lying vibrational states. For the line position analysis, the data set includes infrared and far infrared transitions recorded in this work using high-temperature Fourier transform emission spectroscopy. Also included are already published infrared, far infrared, microwave, terahertz, Doppler-free combination differences, and kHz accuracy lines. The fitting is carried out with the Bending-Rotation approach and allows us to reproduce 12 858 line positions involving levels with $J \leq 20$ and $K_a \leq 18$, with a unitless standard deviation of 1.9, varying 207 spectroscopic parameters. For the line intensity analysis, far infrared line intensities measured in this work using Fourier transform spectroscopy in addition to previously measured line intensities are fitted. 5 612 line intensities are accounted for with a unitless standard deviation of 1.5. The results from both analyses are used to build a line list for atmospherical purposes spanning the 2 to 5000 cm^{-1} spectral range and containing 7 593 lines. This line list as well as calculated energies and line intensities are compared to those already published.

I. INTRODUCTION

As the most abundant isotopic species of water after the main one, the $H_2{}^{18}O$ species is a very important molecule used in many fields, mostly as a tracer. As such, it has been applied to the understanding of the Earth's climate,[1] to assess microbial activity through stable isotope probing,[2] to unravel interstellar water chemistry,[3] and to study terrestrial stratospheric chemistry.[4] In particular, the relationship between $H_2{}^{18}O$ isotopic abundance and the temperature makes this species of particular importance to investigate the climate variability.[5,6] As most of these results are obtained using spectroscopic techniques, very accurate spectroscopic databases should be available for the $H_2{}^{18}O$ species.

The $H_2{}^{18}O$ species, as the main and $H_2{}^{17}O$ isotopologues, is also challenging from the theoretical point of view as it is a nonrigid system displaying a so-called anomalous centrifugal distortion[7] due to the large amplitude nature of its bending mode. For this reason, theoretical approaches designed for semi-rigid molecules, such as the Watson-type Hamiltonian,[8–11] fail to accurately reproduce its energy levels and alternate approaches were developed. These include variational approaches based on *ab initio* calculations,[12–14] fully effective approaches based on experimental energy levels such as those used in the early[15,16] and recent[17,18] high-resolution spectroscopic investigations of water, and the effective 4-D Bending-Rotation approach[19–24] used in the present investigation.

In the current contribution, we present a line position analysis of a large body of data involving the five lowest lying vibrational states of $H_2{}^{18}O$, namely, the (000), (010), (020), (100), and (001) states, where (v_1, v_2, v_3) denotes the vibrational quantum numbers for the symmetrical ν_1 and ν_2 modes at 3649 and 1588 cm^{-1}, respectively, and the asymmetrical ν_3 mode at 3741 cm^{-1}. In addition to available high-resolution measurements, the fitted data contains infrared (IR) and far infrared (FIR) lines retrieved in this work using high temperature emission spectra recorded by Fourier transform spectroscopy (FTS). The fitted data are divided into three sets. The first set includes experimental energy levels; the second one, IR and FIR lines; and the third one, corresponding to highly accurate measurements, includes ground state combination differences[25] microwave (MW) lines,[26–28] terahertz (THz) transitions,[29] and kHz accuracy transitions measured recently.[30] The analysis, carried out with the Bending-Rotation fitting Hamiltonian,[19–24] allows us to reproduce 12 858 data with a unitless standard deviation of 1.9 up to $J = 20$ and $K_a = 18$. The accurate third set of measurements are reproduced with root-mean-square (RMS) deviations ranging from 28 to 315 kHz. A line intensity analysis of absorption transitions involving the same vibrational states is also presented. FIR absorption line intensities measured in this work using FTS were fitted in addition to previously measured line intensities. 5 612 line strengths are accounted for with a unitless standard deviation of 1.5.

[a)] Electronic mail: laurent.coudert@universite-paris-saclay.fr

Combining the line position and line intensity analyses, the present investigation led to a new set of rovibrational levels, line positions, and line intensities and to a new spectroscopic line list up to the First Triad for $H_2{}^{18}O$. The new set of rovibrational levels and line intensities are compared to the so-called W2020 experimental levels of Furtenbacher *et al.*[18] and to the line intensities of Conway *et al.*,[31] respectively. The new database is compared to the line lists built in these two references.

The paper has five remaining sections. Section II is the experimental section where the spectra recorded in this work are presented along with the line assignment procedure. In Section III, theoretical results concerning the Bending-Rotation approach are briefly recalled. The line position and line intensity analyses are carried out in Section IV where the line list is also built. In Section V, comparisons between the results obtained in this work and in previous investigations are performed for the rovibrational energies, line intensities, and the line list. Concluding remarks are given in Section VI.

II. EXPERIMENTAL SPECTRA AND ASSIGNMENT

Both the high-temperature emission and the room-temperature absorption spectra used in this work were recorded by FTS. Throughout the paper, rovibrational levels were assigned using the labeling scheme of Furtenbacher *et al.*[18]

A. High-temperature emission spectra

Line positions were retrieved from four high-temperature emission spectra recorded in different spectral intervals, between 300 and 4500 cm^{-1}, listed in Table I. The I–IV emission spectra were recorded at the Molecular Spectroscopic laboratory of the Justus-Liebig-University (JLU) of Giessen with a Bruker IFS 120 Fourier transform spectrometer.[32] These spectra were obtained as part of a long standing project devoted to the high-resolution spectroscopy of water isotopologues.[33–36] A detailed description of the emission cell as well as other experimental details are given in Ref. 37. As indicated in Table I, Spectra I and II span the rotational range, Spectrum III, the ν_2 band range, and Spectrum IV, the range of the $2\nu_2$, ν_1, and ν_3 interacting bands. Overviews of Spectra I, III, and IV are displayed in Fig. 1 while smaller portions are shown in Fig. 2. The spectral resolution (defined as the inverse of the Maximum Optical Path Difference) varies between 0.005 and 0.015 cm^{-1} while the pressure is in the range 10 to 16 mbar. Estimated values of the temperature range between 1100 and 1680°C.

Note that the isotopic abundance of water vapor strongly varies in the four analyzed spectra: the $H_2{}^{18}O$ relative abundance is close to its normal value, 0.2%, in Spectrum II, but exceeds 50% in the ^{18}O enriched Spectra I and IV. The relative abundances of water isotopologues were estimated by comparison of the line intensities for the same transitions. In Spectrum II, already used in a previous investigation,[38] 90 additional transitions could be assigned for $H_2{}^{18}O$ in the present analysis.

The SyMath SpectrumFit software[39] was used for the line shape fitting and determination of the spectral line parameters. This software allows very accurate line position retrievals in high density spectra with overlapping lines.[37] The $H_2{}^{16}O$ line positions from the W2020 line list[18] were used for the frequency calibration of the four emission spectra.

Altogether, more than 3100 $H_2{}^{18}O$ emission lines were assigned in the four high-temperature emission spectra, from 322 to 4400 cm^{-1}, up to $J = 29$ and $K_a = 18$, in eighteen bands including pure rotational and vibration-rotation (VR) bands. In the sample spectra shown in Fig. 2 the rovibrational assignments are indicated for all water isotopologues. The analysis presented in this work is restricted to transitions with $J \leq 20$ involving the five lowest lying vibrational states. Figure 3 shows schematically the VR levels involved. The line assignment was performed using the variational line lists[40,41] computed by S. A. Tashkun,[42] based on the results of Schwenke and Partridge,[12,43] hereafter referred to as the "SP line lists," and empirical values of VR levels known from previous studies. For assignment purposes, the variational positions of the lines (σ^{SP}) were replaced by their corresponding empirical values (σ^{Emp}) calculated using known empirical energies of the VR levels. The assignment procedure took into account a set of differences between the variational and empirical positions of the lines ($d\sigma = \sigma^{SP} - \sigma^{Emp}$) depending on the rotational numbers J and K_a. As a rule, these $d\sigma$ differences form smooth regular series. In fact, this method allows us to estimate the line positions with an accuracy of a few 10^{-2} cm^{-1}. When possible, the identification of new upper energy levels was supported by the combination difference method (CD) of the lower state energies. Otherwise, in regions with a high density of spectral lines and in the absence of CDs, predictions based on the Bending-Rotation approach were used for the assignments.

B. Fourier transform absorption spectra

For the line intensity measurements, 225 lines assigned to 238 rotational lines within the ground, (010), and (020) vibrational states of $H_2{}^{18}O$ were observed in a far infrared absorption spectrum of water vapor highly enriched in ^{18}O and referred to in Table I as Spectrum V. The spectrum was recorded in the 40–700 cm^{-1} region on the AILES beam line of the SOLEIL synchrotron facility with a water vapor pressure of 4 mbar. Except for the pressure value, the experimental conditions given in Table I were identical to those of the spectrum recorded at 0.97 mbar analyzed by Mikhailenko *et al.*[44] The ^{18}O enrichment of the water sample (from Euriso-

Table I. Experimental conditions of the emission and absorption water spectra recorded at JLU-Giessen and SOLEIL synchrotron, respectively.

Spectrum	Resolution (cm^{-1})	Temperature (°C)	Pressure (mbar)	Range (cm^{-1})	Approximate $H_2{}^{18}O$ abundance in %
			Emission		
I	0.005	1250	15	322–522	>50
II	0.0055	1100	16	380–860	0.2
III	0.005	1303	9.9	1136–1795	∼23
IV	0.015	1680	16	1680–4500	>50
			Absorption		
V	0.00102	23	4	40–700	97

top) was approximately 97%, the absorption pathlength was set to 151.75 m, and the spectral resolution was about 0.001 cm^{-1}. We did not perform a systematic retrieval of the line parameters from the 4 mbar spectrum but focused on newly observed lines or on lines measured with an improved signal-to-noise compared to the 0.97 mbar spectrum of Mikhailenko *et al.*[44] The maximum value of the J and K_a rotational quantum numbers for the transitions assigned in this spectrum are respectively 22 and 14, 17 and 10, and 10 and 6 for rotational transitions assigned within the ground, (010), and (020) vibrational states, respectively.

III. FITTING APPROACH

The Bending-Rotation approach has been used in many investigations of the main[19–24,45,46] and $H_2{}^{18}O$ isotopic species[47] of water, and will be utilized in the present investigation. The success of this approach applied to $H_2{}^{16}O$ has been recently demonstrated by validation tests on the basis of FIR spectra recorded at Synchrotron SOLEIL.[48] The Bending-Rotation approach relies on a simultaneous treatment of the large amplitude bending mode and of the overall rotation. An effective Hamiltonian, based on the exact Hamiltonian of a triatomic molecule written with Radau coordinates,[49,50] is used. This effective Hamiltonian can be applied to any C_{2v} species and depends on various spectroscopic constants to be determined through the fitting of high-resolution spectroscopic data. A first version of the Bending-Rotation approach was developed to deal with the low lying (000) and (010) vibrational states of water.[19–21] A second version allowed us to deal with the higher lying First Triad (020), (100), and (001) and Second Triad (030), (110), and (011) interacting states.[22–24]

In this second version of the Bending-Rotation approach, used in the present investigation, the Schrodinger equation for the bending mode and the overall rotation is solved for each stretching-type state. These states are identified with the integer v which for the present set of states satisfies $0 \leq v \leq 2$. The ground stretching-type state ($v_1 = v_3 = 0$) and first excited symmetrical stretching-type state ($v_1 = 1$ and $v_3 = 0$) correspond to $v = 0$ and 1, respectively. The antisymmetrical excited stretching-type state ($v_1 = 0$ and $v_3 = 1$) corresponds to $v = 2$. The spectroscopic parameters used in the second version involve the kinetic energy constant B_e^v, the potential energy constants V_i^v, with $0 \leq i \leq 6$, and the distortion constants defined in Eq. [33] of Lanquetin *et al.*[22] The Fermi and Coriolis couplings in the First and Second Triads lead to bending-rotational coupling operators between stretching-type states characterized by different values of v. The corresponding coupling constants are B_e^{01}, V_2^{01}, B_e^{02}, B_e^{12}, and the distortion constants in Eqs. [34]–[36] of Lanquetin *et al.*[22] In the present investigation, the bending Hamiltonian matrix is setup using the basis set functions $\theta_n^{\alpha\beta}(t)$ in Eq. (4) of Coudert,[19] with $0 \leq n \leq n_{\rm Max}$, where for each stretching-type state $n_{\rm Max}$ is set to 24. The bending-rotation matrix is setup using 11 (7) bending wavefunctions for the $v = 0$ and 1 ($v = 2$) stretching type-states.

Line strengths can also be computed with the Bending-Rotation approach using a transition moment function[51,52] expanded in terms of bending and rotational operators. This transition moment depends on a set of spectroscopic parameters to be determined through the fitting of experimental line strengths.[20,53] In conjunction with the second version of the Bending-Rotation approach, lines involving any vibrational states up to the Second Triad can be dealt with.[45]

IV. ANALYSES

A. Line position analysis

The fitted data are divided into three sets.

- The first one consists of previously available experimental levels[16,38,54] of the First Triad with $0 \leq J \leq 19$. In order to improve the determination of the bending potentials, the vibrational energy of five states[17] above the First Triad were added to this first set with an experimental uncertainty of 0.005 cm^{-1}.

- The second data set contains the experimental data obtained in this work (Section II A) and previously

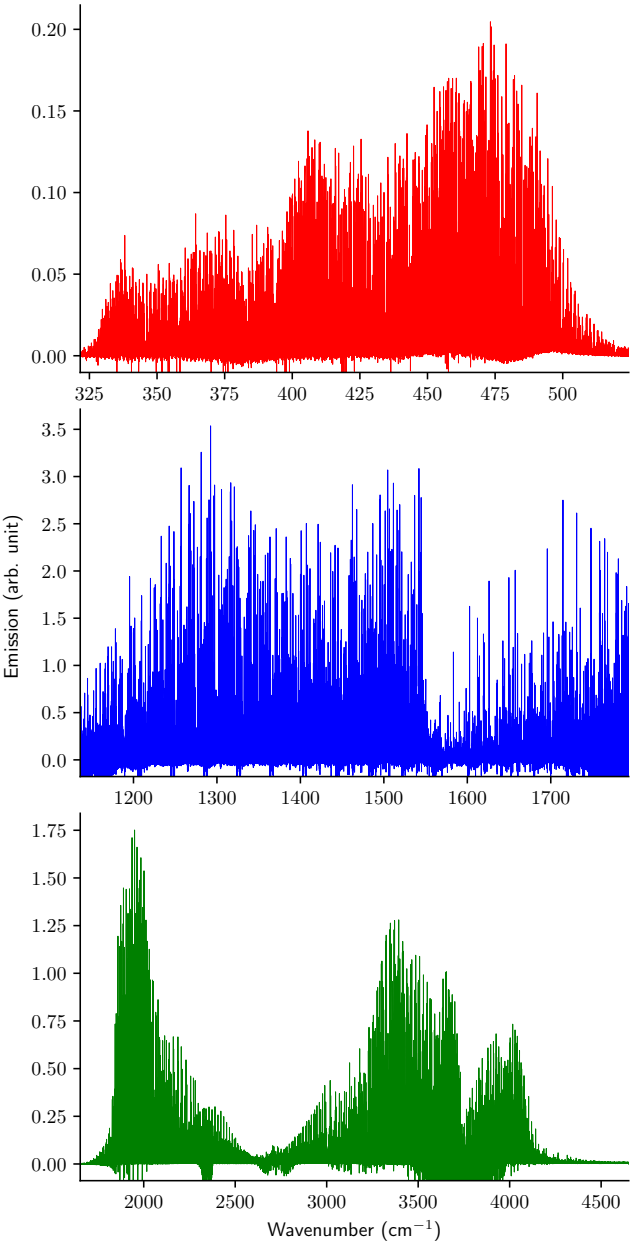

Figure 1. Three emission FTS spectra analyzed in this work. *Upper, middle,* and *lower* panels are Spectra I, III, and IV of Table I, respectively.

published FIR and IR transitions.[16,38,44,54–59] The latter were recorded using either room temperature absorption spectroscopy[16,44,54–59] or high temperature emission spectroscopy.[38] In this second data set, identical transitions reported in different investigations were not removed.

- The third data set includes the most accurate measurements.[25–30] It consists of the microwave measurements of De Lucia *et al.*,[26] Belov *et al.*,[27] and Golubiatnikov *et al.*[28] The data reported by De Lucia *et al.*[26] including the earliest measurements

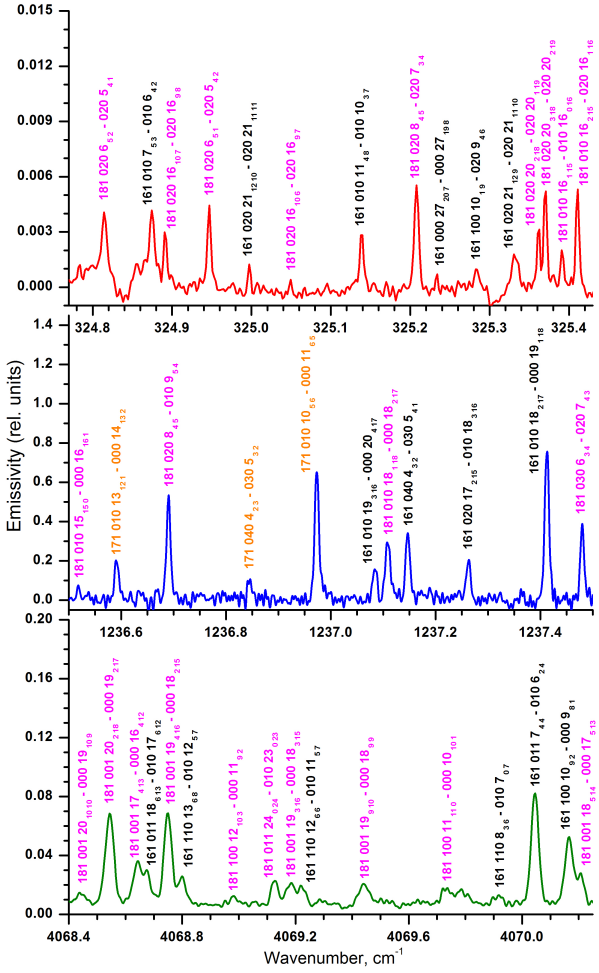

Figure 2. Detailed view of the high-temperature emission FTS spectra analyzed in this work for several narrow spectral intervals. From top to bottom portions of Spectra I, III, and IV, respectively. The assignments are color coded depending on the isotopologue: black for $H_2{}^{16}O$ (label 161), orange for $H_2{}^{17}O$ (171), and pink for $H_2{}^{18}O$ (181).

of Powel *et al.*[60] and Steenbeckeliers and Bellet.[61] This third set also contains the high-accuracy THz frequencies recorded by Matsushima *et al.*,[29] the 9 ground state combination differences obtained by Doppler-free spectroscopy by Gambetta *et al.*,[25] and 124 ground state combination differences extracted from the kHz accuracy transitions measured recently by Diouf *et al.*[30] using the Doppler-free Lamb-dip technique.

Line position data of the three sets were introduced in a weighted least-squares fitting program in which each data point was given a weight equal to the inverse of its experimental uncertainty squared. For the 124 ground state combination differences built from the frequencies reported by Diouf *et al.*,[30] the uncertainty was calculated as the sum of the experimental uncertainty of the two lines used. Unresolved K-type doublets were treated

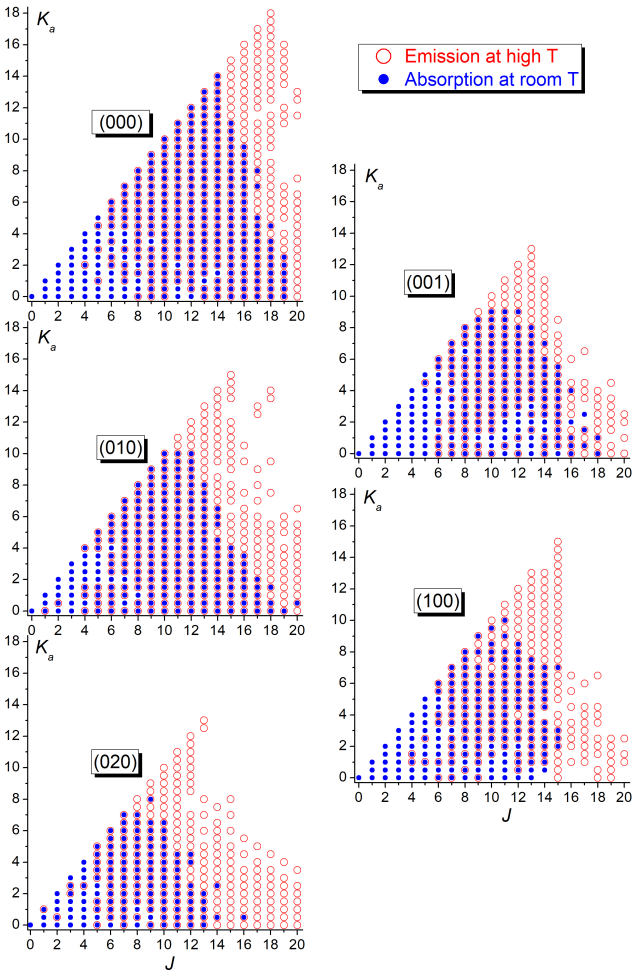

Figure 3. Sets of rotation-vibration $J \leq 20$ levels of the $H_2{}^{18}O$ First Triad used for the present analysis.

as in Section 4 of Coudert.[20] The total number of data is 12 858 for the line position analysis and the unitless standard deviation of the fit is 1.9. The 207 fitted spectroscopic constants are listed in a table available in the supplementary material. The analysis results are described using the RMS deviation of the measured *minus* calculated residuals and the unitless χ^2. This number, referred to as STD in Section 3.2.1 of Coudert *et al.*,[45] should be close to 1 when experimental data are fitted within their stated accuracy. For the three data sets, the results are as follows.

For the first set, analysis results are summarized in Table II for each vibrational state. The five additional vibrational states[17] do not appear explicitly in this table but were taken into account for the first set results given in the last line of the table. 52 energy levels, mostly from Mikhailenko *et al.*[38] and Liu *et al.*,[54] with too large residuals compared to their uncertainty, were excluded from the analysis. For this first data set, the largest residual is 0.056 cm^{-1} for the $19_{1,19}$ (001) rotational level reported in Liu *et al.*[54] with an uncertainty of 0.005 cm^{-1}. Several levels excluded from the previous analysis[47] could be included in the present data set because they were more satisfactorily reproduced. This is the case of the $17_{16,1}$ (000) level displaying a residual of -0.304 cm^{-1} in the previous analysis[47] and of only -0.030 cm^{-1} in the present one. For the second set, the analysis results are reported in Table III for each vibrational band. The number of fitted transitions N given in this table is the actual data number for each vibrational band. Identical transitions reported in different investigations are counted several times. Table IV summarizes the analysis results for the third data set. The THz transitions of Matsushima *et al.*[29] are reproduced slightly more accurately than in the previous analysis[45] since the largest residual decreased from 0.74 MHz to 0.58 MHz. For the 9 frequencies retrieved using Doppler-free spectroscopy by Gambetta *et al.*,[25] the largest residual is 0.07 MHz which is also an improvement compared to that in the previous fit,[45] -0.24 MHz. The kHz accuracy transitions measured by Diouf *et al.*[30] provide us with a test for the accuracy of the present calculation. The 124 ground state combination differences extracted from their measurements could be reproduced with an RMS of 28 kHz. The measured *minus* calculated tables for the three data sets are available in the supplementary material.

Table II. Analysis results for experimental energy levels[a]

State	Reference	J	K_a	N	χ^2
(000)	16 and 38	18	17	304	2.3
(010)	16, 38, and 54	19	11	395	1.9
(020)	54	16	10	141	2.1
(100)	54	15	9	187	1.5
(001)	54	19	9	212	2.4
All	16, 17, 38, and 54	19	17	1244	2.0

[a] The reference from which experimental energies were taken, the maximum J- and K_a-values, the number of fitted levels N, and the value of χ^2 are given for each state.

The results of the line position analysis are summarized by reference in Table V. For each transition i, the unitless ratio $r_i = \Delta_i/u_i$ was computed, where Δ_i is the measured *minus* calculated residual and u_i is the total uncertainty evaluated as the experimental one plus that of the calculated line position. The latter is retrieved from the covariance matrix as outlined in Section IV C. For each reference, Table V lists the average value of $|r_i|$, its maximum value, the number of transitions with $|r_i| > 1$, that with $|r_i| > 5$, and the unitless χ^2. In the case of a satisfactory analysis, the average and maximum value of $|r_i|$ are expected to be close to 1 and there should be no transition with $|r_i| > 1$ and $|r_i| > 5$. Table V emphasizes that the data from Refs. 27, 30, 38, and 59 were reported with too small experimental uncertainties. For the Lamb-Dip measurements of Diouf *et al.*,[30] it should be pointed out the unsatisfactory results are not due to the fitting approach since this data set involves transitions with a low maximum J-value of 11.

Table III. Analysis results for IR and FIR transitions[a]

Band[b]	Reference	J	K_a	N	χ^2
(000)	*This work,* 38, 44, 54–56	20	18	758	1.9
ν_2	*This work,* 16, 54, 56, and 59	20	16	2881	1.2
(010)	*This work,* 38 and 44	20	13	499	1.3
$2\nu_2$	*This work,* 54, 57, and 59	19	11	1174	2.5
$2\nu_2 - \nu_2$	*This work,* 54, 56, 57, and 59	20	14	1214	1.9
(020)	*This work,* 44	20	10	151	2.9
$2\nu_2 - \nu_1$	*This work*	14	10	18	3.0
ν_1	*This work,* 54, 58, and 59	20	16	1621	2.0
$\nu_1 - \nu_2$	*This work,* 54 and 56	15	11	310	1.3
$\nu_1 - 2\nu_2$	*This work*	13	12	16	4.1
(100)	*This work*	20	11	126	3.5
$\nu_1 - \nu_3$	*This work*	13	6	9	0.8
ν_3	*This work,* 54, 58, and 59	20	14	2088	1.8
$\nu_3 - \nu_2$	*This work,* 54 and 56	20	9	310	1.3
$\nu_3 - \nu_1$	*This work*	15	8	14	0.9
(001)	*This work*	20	11	144	1.8
All	*This work* (Section II A)	20	18	2730	2.6
All	*This work,* 16, 38, 44, 54–59	20	18	11332	1.8

[a] The reference from which experimental wavenumbers were taken, the maximum J- and K_a-values, the number of fitted transitions N, and the value of χ^2 are given for each band. An additional row lists these results only for transitions measured in this work, reported in Section II A.

[b] The band name is given in this column. A vibrational state label indicates pure rotational transitions within that state.

Table IV. Analysis results for the third data set[a]

Data type	State	J	K_a	N	RMS	χ^2
Microwave[26–28]	(000) and (010)	11	7	23	315	1.9
Terahertz[29]	(000)	10	7	118	149	2.3
Doppler-Free[25]	(000)	5	3	9	41	0.5
Lamb-Dip[30]	(000)	11	8	124	28	4.6
All[25–30]	(000) and (010)	11	8	274	135	3.5

[a] Data type, vibrational state, maximum J- and K_a-values, number of fitted transitions N, RMS in kHz, and χ^2 are given.

B. Line strength analysis

The line intensities measured in this work, presented in Section II B, and previously published line intensities[16,44,56–59,62,63] were analyzed computing the intensity as indicated in Section 4 of Coudert *et al.*[45] The eigenvectors needed to evaluate the transition moment matrix elements, the transition wavenumber, and the lower level energy were taken from the line position analysis. A weight equal to the inverse of the experimental uncertainty squared was used for each data point. The strength of transitions corresponding to unresolved K-type doublets was calculated as in Section 4.2 of Coudert *et al.*[45]

In the analysis, line intensities were normalized to 100% of $H_2{}^{18}O$. The line strengths reported in Refs. 16, 44, 57, and 58 were included in the data set with no change. The line strengths reported by Winther[62] were multiplied by 500 since his measurements are for $H_2{}^{18}O$ in natural isotopic abundance. The experimental uncertainties, not given explicitly by Winther, were taken to be 10% divided by the square root of the weight given by the author in his Table I. For the line strengths reported by Oudot *et al.*,[56] the same multiplying factor was used in agreement with their Table 9. For the line strengths reported by Toth,[63] a calibration factor of 500 was also used as his measurements appear to correspond to $H_2{}^{18}O$ in natural isotopic abundance. For the relative line strengths reported by Loos *et al.*,[59] a calibration factor of 510 was found with the help of the previous measurements and is also consistent with $H_2{}^{18}O$ in natural isotopic abundance. 5 612 line strengths were fitted, 105 spectroscopic parameters were varied, and the unitless standard deviation is 1.5. The measured *minus* calculated table is available in the supplementary material. Table VI summarizes the results of the analysis for each band and Fig. 4 displays the line strength residuals as a function of the observed line strength. 21 outliers with an intensity residual between 50% and 73% of their observed intensity are not shown.

Table V. Analysis results by reference[a]

Reference	N	$\bar{r}$	r_{Max}	N_1	N_5	χ^2
26	9	0.2	0.5	0	0	0.2
25	9	0.3	0.8	0	0	0.5
44	732	0.4	4.7	67	0	0.9
56	1584	0.5	9.9	194	6	0.9
16	751	0.6	3.8	139	0	1.1
54	2905	0.6	6.8	449	9	1.1
55	33	1.0	4.1	10	0	1.3
58	998	0.6	4.9	174	0	1.3
57	457	0.9	4.5	159	0	1.8
28	6	0.7	1.6	2	0	2.0
29	118	1.4	8.8	60	3	2.3
This work	2730	1.0	8.3	942	27	2.6
27	8	1.0	1.9	4	0	2.7
59	1023	1.2	7.2	512	10	2.8
38	119	1.3	9.6	61	2	3.3
30	124	1.3	3.7	67	0	4.6

[a] The reference from which the experimental line positions were taken, the number of fitted transitions N, $\bar{r}$ the average value of $|r_i|$, its maximum value r_{Max}, N_1 the number of transitions with $|r_i| > 1$, N_5 that with $|r_i| > 5$, and the value of χ^2 are given. The unitless r_i is defined in Section IV A. References are listed with increasing value of χ^2.

When compared to Fig. 1 of Coudert and Chélin,[47] Fig. 4 of the present paper seems to imply that the results of the present line intensity analysis are much worse than those of the previous one. Although the unitless standard deviations of both analyses are nearly equal, the present one is more satisfactory since 1.5 times more data were considered. The differences between both figures stem mainly from the fact that the present data set includes more lines characterized by a large intensity uncertainty than in Coudert and Chélin.[47]

Table VI. Line strength analysis results[a]

Band[b]	Reference	J	K_a	N	χ^2
(000)	*This work,* 44, 56, 62, and 63	20	14	655	1.4
ν_2	16, 56, and 59	18	11	1787	1.5
(010)	*This work,* 44	17	10	333	1.5
$2\nu_2$	57 and 59	13	7	534	1.2
$2\nu_2 - \nu_2$	56, 57, and 59	14	7	440	1.5
(020)	*This work,* 44	10	6	26	2.6
ν_1	58 and 59	14	9	704	1.5
$\nu_1 - \nu_2$	56	10	7	93	2.4
ν_3	58 and 59	16	8	945	1.3
$\nu_3 - \nu_2$	56	10	6	97	1.9
All	*This work* (Section II B)	20	14	211	1.6
All	*This work,* 16, 44, 56–59, 62, and 63	20	14	5612	1.5

[a] The reference from which experimental line intensities were taken, the maximum J- and K_a-values, the number of fitted transitions N, and the value of χ^2 are given for each band. An additional row lists these results only for transitions measured in this work, reported in Section II B.

[b] The band name is given in this column. A vibrational state label indicates pure rotational transitions within that state.

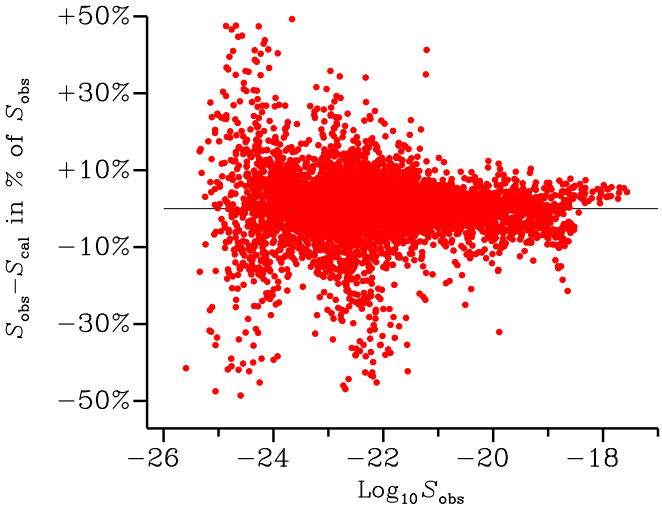

Figure 4. Residuals $S_{obs} - S_{cal}$, in percent of the measured line strength S_{obs}, for the line intensity analysis. The abscissa is the base 10 logarithm of the observed line strength in cm/molecule. 16 outliers with $|S_{obs} - S_{cal}|$ between 50% and 80% of S_{obs} are not shown.

C. Line position and line strength database

A line list spanning the spectral range 2 to 5000 cm^{-1} was built using the results of the line position and line strength analyses. A maximum J-values of 21 and an intensity cutoff of 10^{-28} cm/molecule were taken for a temperature of 296 K and an isotopic abundance[64] of 0.00199983. The cutoff value is consistent with the fact that lines involving vibrational states beyond the First Triad or a J-value larger than 21 are missing from the present line list and are expected to have an intensity on the order of 10^{-28} cm/molecule or slightly larger. The database contains 7 593 lines and is formatted as a HITRAN line list.[64] No efforts were made to estimate the value of the line shape parameters which were set to zero as well as the line strength errors. The line position error parameters were set to the appropriate value[64] using the calculated line position uncertainty as retrieved below. The database is available in the supplementary material.

A list of calculated levels with assignments, energies, and energy uncertainties is also available in the supplementary material. This list was computed from the line position analysis results and uncertainties were estimated using the covariance matrix. The selected levels include those involved in the line position analysis data set. The reliability of the calculated uncertainties was checked making sure that, for the most accurate transitions in the line position analysis data set, the calculated uncertainty exceeds the experimental one. The most accurate transitions in the line position data set are 6 ground state combination differences[30] characterized by an experimental uncertainty of 3.6 kHz and their calculated line incertainties range from 4.9 to 10 kHz.

V. COMPARISONS

A. Energy levels

The so-called W2020 energy levels of Furtenbacher *et al.*[18] were compared to those obtained in the line position analysis of Section IV A. The comparison was restricted to levels with $J \leq 20$, which is the maximum value of J in the analysis. For each level i of Furtenbacher *et al.*,[18] the unitless ratio $r_i = \Delta_i/u_i$ was calculated, where Δ_i is the difference between the energy reported by these authors and that from this work and u_i is the total uncertainy equal to the W2020 uncertainty plus that retrieved in this work. Figure 5 shows this ratio as a function of the level energy. As can be gathered from this figure, only 42% W2020 energy levels display a residual within the total uncertainty ($|r_i| < 1$). The largest r_i value is observed for the $12_{10,3}, (001)$ level reported at 6873.2595 cm^{-1} by Furtenbacher *et al.*[18] and calculated in this work at 6871.8445 cm^{-1}. The $12_{10,3}$ and $12_{10,2}(001)$ levels, being the two members of a $K_a = 10$ asymmetry doublet, are expected to be nearly degenerate. Indeed the asymmetry splitting calculated in this work is about 0.001 cm^{-1} while that in Furtenbacher *et al.*[18] exceeds 1 cm^{-1}. The large r_i can be attributed to the way the energy of these levels were retrieved. No experimental transitions involving the $12_{10,3}$ and $12_{10,2}(001)$ levels being available, the W2020 energy values actually come from a calculated line list[47] where the former level was misassigned. Figure 5 is consistent with a good agreement for levels belonging to the ground vibrational state although there seems to be a systematic negative trend for energies below 1000 cm^{-1}.

The large number of levels with a ratio $|r_i| > 1$ may be attributed to the differences between the energy level

based analysis of Furtenbacher *et al.*[18] and the model based fitting procedure used in this work. In an energy level based analysis, the parameters fitted to the line position are the energies of the levels and there may be many of these, in some cases, more than several thousand. In the fitting approach used in this work, the parameters fitted to the line position have a physical meaning and their number, usually much smaller, is equal to 207 in the present investigation. With our approach, an averaging takes place which greatly reduces parameter uncertainties and leads to energies with a much smaller uncertainty than with a level based analysis.

The experimental wavenumbers of the previously published FIR and IR transitions,[16,38,44,54–59] considered in the line position analysis of Section IV A, were computed using the W2020 energy values.[18] Table VII, organized as Table III, summarizes the comparison results. In the case of the ν_1 and ν_2 fundamental bands, observed wavenumbers are better reproduced with the levels of Furtenbacher *et al.*[18] than in the present work; for ground vibrational state transitions and for the fundamental ν_3 band, it is just the opposite. For ground vibrational state transitions, the largest residual compared to Furtenbacher *et al.*[18] is -0.031 cm^{-1} for the $19_{2,17} \leftarrow 18_{3,16}$ transition measured at 388.8338 cm^{-1} by Mikhailenko *et al.*[44] using room temperature absorption spectroscopy. Since its reported experimental uncertainty is 0.0001 cm^{-1}, this leads to the large χ^2 of 3.1 for W2020. Our Meas. – Calc. residual for this transition is 0.00051 cm^{-1}.

The even larger χ^2 value listed in this table with the W2020 levels for the ν_3 band is due to an even larger maximum residual of 0.239 cm^{-1} arising for the $11_{11,1} \leftarrow 11_{11,0}$ transition reported at 3624.3967 cm^{-1} by Liu *et al.*[54] and characterized by an experimental uncertainty of 0.001 cm^{-1}. Our Meas. – Calc. residual is 0.003 cm^{-1} for this transition while the W2020 residual significantly exceeds the W2020 upper and lower levels uncertainties, respectively 1.016×10^{-3} and 7.49×10^{-5} cm^{-1}. This situation results from the fact that the 3624.3967 cm^{-1} transition[54] was not used by Furtenbacher *et al.*[18] to retrieve the energy of the $11_{11}(001)$ level. These authors relied on a calculated line list[47] where this transition, characterized by a large K_a-value, was not accurately predicted.

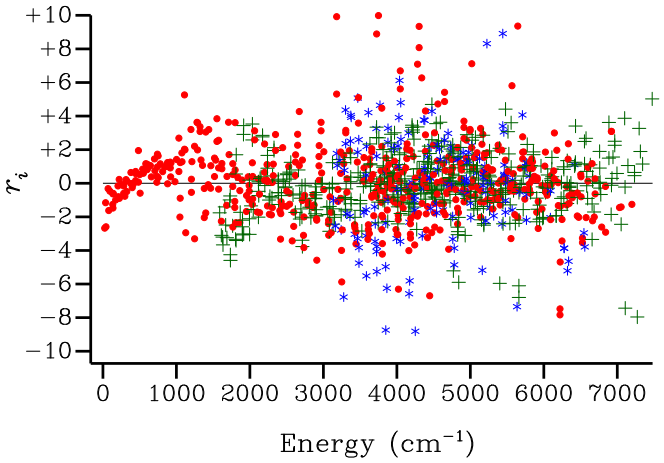

Figure 5. The unitless ratio r_i, which compares the deviation of W2020 energy values[18] from our computed energy values scaled by the total uncertainty, as a function of the level energy in cm^{-1}. Full circles, plus signs (+), and stars (*) are used for levels belonging respectively to the ground, (010), and First Triad states. 50 outliers with $|r_i| > 10$ are not shown.

Table VII. Line position residuals[a] with Ref. 18 and this work

		Ref. 18		*This work*	
Band[b]	Reference	N	χ^2	N	χ^2
(000)	38, 44, 54–56	558	3.1	559	1.8
ν_2	16, 54, 56, and 59	2433	0.7	2434	1.0
(010)	38 and 44	321	0.6	323	0.7
$2\nu_2$	54, 57, and 59	1089	2.9	1092	2.2
$2\nu_2 - \nu_2$	54, 56, 57, and 59	766	0.7	766	0.9
(020)	44	22	0.6	22	1.1
ν_1	54, 58, and 59	1317	1.1	1315	1.6
$\nu_1 - \nu_2$	54 and 56	235	1.1	235	1.1
ν_3	54, 58, and 59	1658	5.9	1658	1.6
$\nu_3 - \nu_2$	54 and 56	199	1.3	199	1.3
All	16, 38, 44, 54–59	8597	3.0	8602	1.5

[a] This table is organized as Table III and, for each vibrational band of the previously published FIR and IR experimental transitions considered in the line position analysis, compares the number of transitions considered, N, and the value of χ^2 obtained with the W2020 levels[18] and in this work.

[b] The band name is given in this column. A vibrational state label indicates pure rotational transitions within that state.

B. Line strengths

The calculated line strengths reported by Conway *et al.*[31] are compared to the previously published experimental line intensities[16,44,56–59,62,63] considered in the line strength analysis of Section IV B. Table VIII compares the residuals obtained with the line list of Conway *et al.*[31] and those obtained in this work. For almost all vibrational bands, the χ^2 values obtained in the present investigation are more satisfactory.

C. Line lists

The line list built by Conway *et al.*[31] and the so-called W2020 line list of Furtenbacher *et al.*[18] were compared to that built in this work. The list of Conway *et al.* is the main source of HITRAN2020[64] intensities in our region while most of the HITRAN2020 line positions were taken from the W2020 line list.

Table VIII. Line strength residuals[a] with Ref. 31 and this work

		Ref. 31		*This work*	
Band[b]	Reference	N	χ^2	N	χ^2
(000)	44, 56, 62, and 63	485	1.4	537	1.4
ν_2	16, 56, and 59	1731	1.6	1787	1.5
(010)	44	240	1.4	247	1.4
$2\nu_2$	57 and 59	531	1.7	534	1.2
$2\nu_2 - \nu_2$	56, 57, and 59	434	1.6	440	1.5
(020)	44	18	3.0	18	3.0
ν_1	58 and 59	690	3.1	704	1.5
$\nu_1 - \nu_2$	56	92	3.6	93	2.4
ν_3	58 and 59	920	2.0	945	1.3
$\nu_3 - \nu_2$	56	96	3.6	97	1.9
All	16, 44, 56–59, 62, and 63	5237	2.0	5401	1.5

[a] For the previously published experimental line intensities considered in the line strength analysis, this table, organized as Table VI, compares for each vibrational band the number of transitions considered N and the value of χ^2 obtained using the results of Conway *et al.*[31] and those in Section IV B.

[b] The band name is given in this column. A vibrational state label indicates pure rotational transitions within that state.

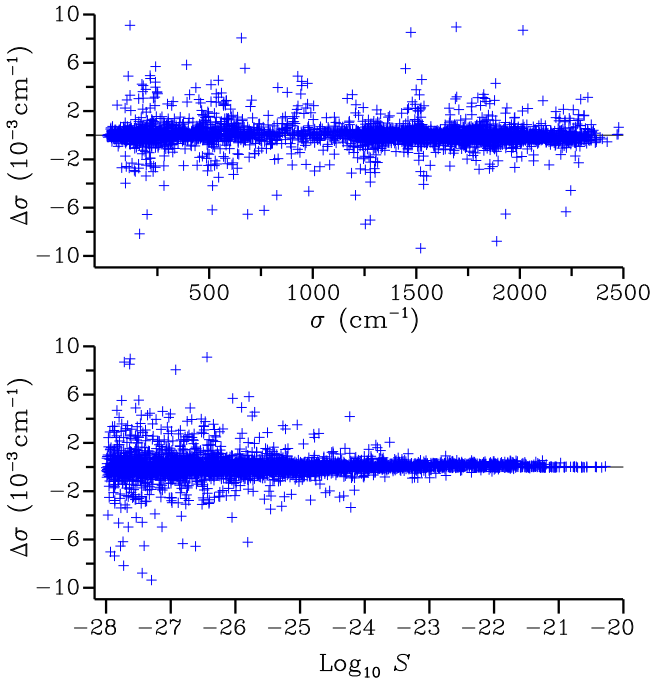

Figure 6. For the 3 974 common lines in the 2 to 2500 cm^{-1} range with a line strength larger than 10^{-28} cm/molecule listed both in Conway *et al.*[31] and in the database built in this work, the line position difference $\Delta\sigma = \sigma$(Ref. 31) − σ(This work) is plotted as a function of the wavenumber (line strength) in the upper (lower) panel. Line strengths include the isotopic abundance factor. 41 outliers do not appear in this figure.

1. Conway et al.[31]

In the line list of Conway *et al.*,[31] transitions listed twice with exactly the same assignment, wavenumber, and intensity were found. For instance, the $3_{22} \leftarrow 2_{11}$ rotational transition of (010) at 118.8435 cm^{-1} appears twice. The number of such pairs amounts to 100 for the line set considered below and the second instance was ignored. Misassigned lines were also ignored.

The first comparison is for line positions and is restricted to transitions with a wavenumber in the range 2 to 2500 cm^{-1}, a strength larger than 10^{-28} cm/molecule, including the isotopic abundance factor, and a J-value smaller than 20. The number of such lines is 4 029 for Conway *et al.*[31] and 4 157 for our database. There are 3 974 lines with identical rovibrational assignment, listed in both databases. For these lines, Fig. 6 displays the line position difference $\Delta\sigma = \sigma$(Ref. 31) − σ(This work) plotted against the line wavenumber and intensity. This figure emphasizes that the largest discrepancies are observed for weak lines with a strength smaller than 10^{-24} cm/molecule. These large discrepancies are evenly scattered in the 2 to 2500 cm^{-1} range. 41 outliers do not appear in Fig. 6 because they display discrepancies larger than 0.01 cm^{-1}. The largest discrepancy is 0.0788 cm^{-1} for the $2\nu_2 - \nu_2$ band $11_{5,6} \leftarrow 10_{4,7}$ transition with position and strength calculated in this work to be 2065.8758 cm^{-1} and 1.3×10^{-28} cm/molecule. The strongest outlier is the ground vibrational state $16_{3,14} \leftarrow 15_{2,13}$ transition displaying a discrepancy of −0.0238 cm^{-1} and with position and strength calculated in this work to be 337.4224 cm^{-1} and 1.36×10^{-25} cm/molecule. The RMS of the residuals is 0.0028 cm^{-1} for the 3 974 common lines and 0.0009 cm^{-1} ignoring 41 outliers. 183 lines of the database computed in this work could not be found in Conway *et al.*[31] Their strength ranges from 10^{-28} to 1.63×10^{-25} cm/molecule. Conversely, 55 transitions of Conway *et al.*[31] could not be found in our list, their strengths ranging from 10^{-28} to 2.82×10^{-28} cm/molecule are close to our intensity cutoff.

The second comparison is for line intensities. Transitions are selected as for the previous comparison but the wavenumber range is 2500 to 4500 cm^{-1}. The number of lines fulfilling these criteria is 3 263 for Conway *et al.*,[31] and 3 417 for our database. There are 3 141 common lines in this range and the corresponding plots against the line wavenumber and intensity are displayed in Fig. 7. A clear systematic shift by about 3 to 4% is observed for the line intensities, our values being larger than those of Conway *et al.*[31] The RMS of the residuals is 40% for the 3 141 common lines and 9.8% ignoring 212 outliers.

2. W2020 line list[18]

In the comparisons below, partially assigned lines were skipped in the Furtenbacher *et al.*[18] line list. The first comparison, for line strengths, was carried out in the range 2 to 2500 cm^{-1} with the same restrictions as in

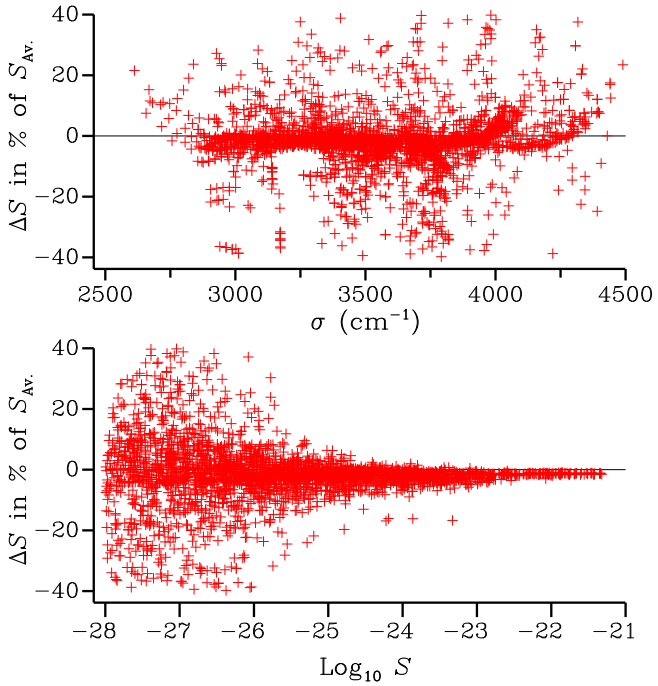

Figure 7. For the 3 141 common lines in the range 2500 to 4500 cm^{-1} with a line strength larger than 10^{-28} cm/molecule listed both in Conway *et al.*[31] and in the database built in this work, the line strength difference $\Delta S = S(\text{Ref. 31}) - S(\text{This work})$ in % of the average strength $S_{\text{Av.}} = [S(\text{Ref. 31}) + S(\text{This work})]/2$ is plotted as a function of the wavenumber (line strength) in the upper (lower) panel of the figure. Line strengths include the isotopic abundance factor. 212 outliers do not appear in this figure.

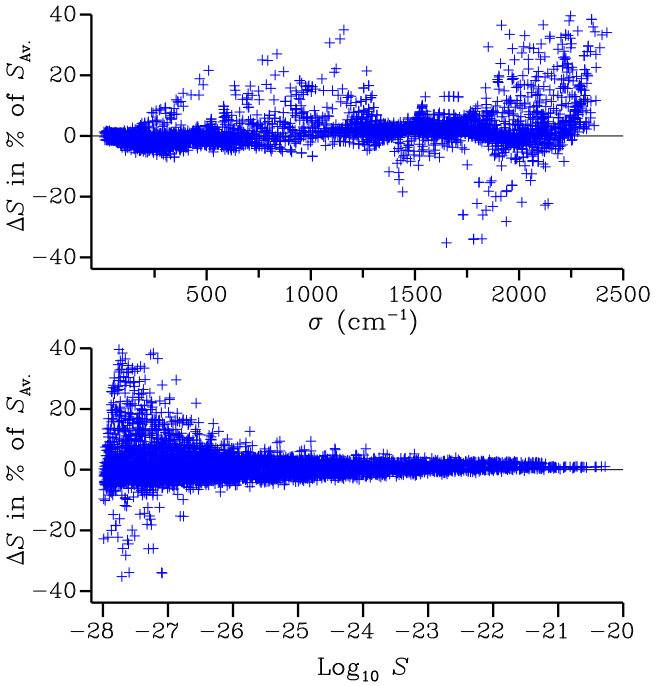

Figure 8. For the 4 085 common lines in the range 2 to 2500 cm^{-1} with a line strength larger than 10^{-28} cm/molecule listed both in Furtenbacher *et al.*[18] and in the database built in this work, the line strength difference $\Delta S = S(\text{Ref. 18}) - S(\text{This work})$ in % of the average strength $S_{\text{Av.}} = [S(\text{Ref. 18}) + S(\text{This work})]/2$ is plotted as a function of the wavenumber (line strength) in the upper (lower) panel. Line strengths include the isotopic abundance correction of Section IV C. 20 outliers do not appear in this figure.

Section V C 1. The number of lines fulfilling these criteria is 4 141 for Furtenbacher *et al.*[18] and 4 204 for our database. There are 4 085 common lines and the corresponding plots against the line wavenumber and intensity are displayed in Fig. 8. There is a good agreement between both line lists. The largest discrepancies are observed in the ν_2 band region for weak transitions with a strength smaller than 10^{-26} cm/molecule. The RMS of the residuals is 7.5% for the 4 085 common lines and 6.2% ignoring 20 outliers.

The second comparison, for line positions, was performed in the range 2500 to 4500 cm^{-1} with the same restrictions as in Section V C 1. There are 3 163 common lines listed in both databases. Figure 9 displays the line position difference $\Delta\sigma = \sigma(\text{Ref. 18}) - \sigma(\text{This work})$ plotted against the line wavenumber and intensity; the latter including the isotopic abundance factor. This figure emphasizes that the largest discrepancies are observed for weak lines with a strength smaller than 10^{-24} cm/molecule. These large discrepancies are evenly scattered in the 2500 to 4500 cm^{-1} range. 82 outliers do not appear in Fig. 9 because they display discrepancies larger than 0.01 cm^{-1}. The largest discrepancy is 0.2747 cm^{-1} for the ν_1 band $10_{10,1} \leftarrow 10_{9,2}$ transition with position and strength calculated in this work to be 3776.5875 cm^{-1} and 1.9×10^{-28} cm/molecule. The RMS of the residuals is 0.0116 cm^{-1} for the 3 163 common lines and 0.0009 cm^{-1} ignoring the 82 outliers. 172 lines of the database computed in this work could not be found in Furtenbacher *et al.*[18] Their strength ranges from 10^{-28} to 2.5×10^{-27} cm/molecule. Conversely, 54 transitions of Furtenbacher *et al.*[18] could not be found in our list. Their strengths range from 10^{-28} to 5.6×10^{-28} cm/molecule.

VI. CONCLUDING REMARKS

The present paper reports new measurements in the $H_2{}^{18}O$ species FIR and IR high-resolution spectra recorded using high-temperature emission and room-temperature absorption FTS. The results of line position and line intensity analyses are also reported for transitions involving the (000), (010), (020), (100), and (001) vibrational states. The main outcome of the present investigation is a HITRAN type line list[64] built using both analyses results.

The data considered in the line position analysis involve the new lines recorded in this work, already published FIR and IR measurements, and highly accurate measurements consisting of ground state combi-

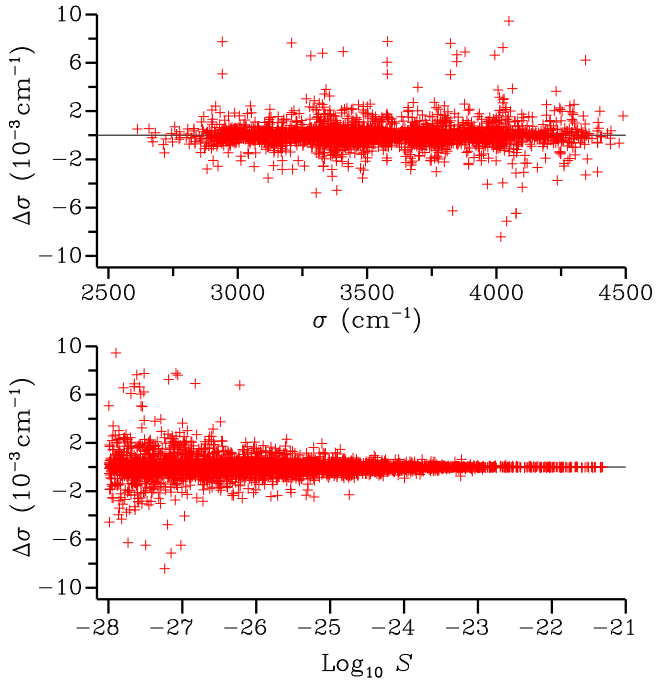

Figure 9. For the 3 163 common lines in the 2500 to 4500 cm^{-1} range with a line strength larger than 10^{-28} cm/molecule listed both in Furtenbacher *et al.*[18] and in the database built in this work, the line position difference $\Delta\sigma = \sigma$(Ref. 18) − σ(This work) is plotted as a function of the wavenumber (line strength) in the upper (lower) panel. Line strengths include the isotopic abundance factor. 82 outliers do not appear in this figure.

nation differences,[25] microwave,[26–28] THz transitions,[29] and kHz accuracy transitions.[30] The spectral modeling was carried out with the Bending-Rotation fitting Hamiltonian.[19–24] 12 858 data are accounted for with a unitless standard deviation of 1.9 up to $J = 20$ and $K_a = 18$. As emphasized by Table IV, the highly accurate data are satisfactorily reproduced. In particular, for the recent Lamb-dip measurements of Diouf *et al.*,[30] a value of 28 kHz was obtained for the RMS deviation of the frequency residuals. Table V, where the analysis results are listed by references, reveals that the experimental line uncertainties reported in several investigations are too small. This leads to an unitless standard deviation which is much larger than 1 in the line position analysis.

The data considered in the line intensity analysis consist of the new line strengths measured in this work and of previously published line intensities. 5 612 line strengths are accounted for with a unitless standard deviation of 1.5. Table VI reveals that for the 10 fitted vibrational bands, the value of χ^2 is at most 2.6.

The energy level values deduced from the line position analysis were compared to the W2020 empirical values of Furtenbacher *et al.*[18] The comparison results are given in Section V A. Figure 5 emphasizes that the discrepancies between the W2020 levels and those of the present work tend to exceed a total uncertainty equal to the quoted W2020 uncertainty plus that estimated in this work. Table VII reveals that when used to compute the measured line positions of already published FIR and IR transitions,[16,38,44,54–59] the value of χ^2 with the energy levels of Furtenbacher *et al.*[18] varies from 0.6 to 3.1 depending on the vibrational band. For all transitions, the unsatisfactory χ^2 value of 3.0 obtained for the W2020 line positions is due to a few erroneous wavenumbers. Similarly, for line intensities, Table VIII emphasizes that those reported by Conway *et al.*[31] do not reproduce quite accurately the experimental values[16,44,56–59,62,63] used to derive our effective transition moment operator in Section IV B. This is an important outcome since the intensity values computed by Conway *et al.*[31] are the main source of line intensity adopted in the HITRAN2020 database[64] in our region.

In Section V C, the line lists built by Conway *et al.*[31] and Furtenbacher *et al.*[18] are compared to that generated in this work. As illustrated in Figs. 6–8, the discrepancies for line positions and line intensities can be large in the case of weak lines.

VII. SUPPLEMENTARY MATERIAL

Observed *minus* calculated tables for each data set considered in the line position analysis are available along with a table containing the fitted spectroscopic parameters. The observed *minus* calculated table for the line intensity analysis is also available along with the Hitran-type database and an energy level list.

VIII. DATA AVAILABILITY STATEMENT

The data that support the findings of this study are available within the article and its supplementary material.

ACKNOWLEDGEMENTS

Financial support from the CNRS (France) in the frame of the International Research Project (SAMIA) and from the Ministry of Science and Higher Education of the Russian Federation (V. E. Zuev Institute of Atmospheric Optics, SB, RAS) is gratefully acknowledged. The authors are indebted to T. A. Odintsova, M. Yu. Tretyakov, and O. Pirali for recording the FIR spectrum of $H_2{}^{18}O$ at Synchrotron SOLEIL (Project number 20180347).

[1] M. Werner, B. Haese, X. Xu, X. Zhang, M. Butzin, and G. Lohmann, "Glacial–interglacial changes in $H_2{}^{18}O$, HDO and deuterium excess – results from the fully coupled ECHAM5/MPI-OM Earth system model," Geoscientific Model Dev. **9**, 647–670 (2016).

[2]K. Papp, R. L. Mau, M. Hayer, B. J. Koch, B. A. Hungate, and E. Schwartz, "Quantitative stable isotope probing with $H_2{}^{18}O$ reveals that most bacterial taxa in soil synthesize new ribosomal rna," ISME J. **12**, 3043–3045 (2018).

[3]E. F. van Dishoeck, E. Herbst, and D. A. Neufeld, "Interstellar water chemistry: From laboratory to observations," Chem. Rev. **113**, 9043–9085 (2013).

[4]M. T. Coffey, J. W. Hannigan, and A. Goldman, "Observations of upper tropospheric/lower stratospheric water vapor and its isotopes," J. Geophys. Res. **111**, D14313 (2006).

[5]J. Jouzel, G. L. Russell, R. J. Suozzo, R. D. Koster, J. W. C. White, and W. S. Broecker, "Simulations of the HDO and $H_2{}^{18}O$ atmospheric cycles using the NASA GISS general circulation model: The seasonal cycle for present-day conditions," J. Geophys. Res. **92**, 14739–14760 (1987).

[6]M. Werner, J. Jouzel, V. Masson-Delmotte, and G. Lohmann, "Reconciling glacial antarctic water stable isotopes with ice sheet topography and the isotopic paleothermometer," Nature Comm. **9**, 3537–3547 (2018).

[7]C. Camy-Peyret and J.-M. Flaud, "The interacting states (030), (110), and (011) of $H_2{}^{16}O$," J. Mol. Spectrosc. **59**, 327–337 (1976).

[8]J. K. G. Watson, "Determination of Centrifugal-Distortion Coefficients of Asymmetric-Top Molecules," J. Chem. Phys. **46**, 1935–1949 (1967).

[9]J. K. G. Watson, "Determination of Centrifugal-Distortion Coefficients of Asymmetric-Top Molecules. II. Dreizler, Dendl, and Rudolph's Results," J. Chem. Phys. **48**, 181–185 (1968).

[10]J. K. G. Watson, "Determination of Centrifugal-Distortion Coefficients of Asymmetric-Top Molecules. III. Sextic Coefficients," J. Chem. Phys. **48**, 4517–4524 (1968).

[11]J. K. G. Watson, in *"Vibrational Spectra and Structure" Vol. 6, page 1*, edited by J. R. Durig (Elsevier, Amsterdam, 1977).

[12]H. Partridge and D. W. Schwenke, "The determination of an accurate isotope dependent potential energy surface for water from extensive ab initio calculations and experimental data," J. Chem. Phys. **106**, 4618–4639 (1997).

[13]R. J. Barber, J. Tennyson, G. J. Harris, and R. N. Tolchenov, "A high-accuracy computed water line list," Mon. Not. R. Astron. Soc. **368**, 1087–1094 (2006).

[14]O. L. Polyansky, A. A. Kyuberis, N. F. Zobov, J. Tennyson, S. N. Yurchenko, and L. Lodi, "Exomol molecular line lists XXX: a complete high-accuracy line list for water," Mon. Not. R. Astron. Soc. **480**, 2597–2608 (2018).

[15]C. Camy-Peyret, J.-M. Flaud, J.-P. Maillard, and G. Guelachvili, "Higher ro-vibrational levels of H_2O deduced from high resolution oxygen-hydrogen flame spectra between 6200 and 9100 cm^{-1}," Mol. Phys. **33**, 1641–1650 (1977).

[16]R. A. Toth, "Transition frequencies and absolute strengths of $H_2{}^{17}O$ and $H_2{}^{18}O$ in the 6.2-μm region," J. Opt. Soc. Am. B **9**, 462–482 (1992).

[17]J. Tennyson, P. F. Bernath, L. R. Brown, A. Campargue, M. R. Carleer, A. G. Császár, R. R. Gamache, J. T. Hodges, A. Jenouvrier, O. V. Naumenko, O. L. Polyansky, L. S. Rothman, R. A. Toth, A. C. Vandaele, N. F. Zobov, L. Daumont, A. Z. Fazliev, T. Furtenbacher, I. E. Gordon, S. N. Mikhailenko, and S. V. Shirin, "IUPAC critical evaluation of the rotational-vibrational spectra of water vapor. Part I–Energy levels and transition wavenumbers for $H_2{}^{17}O$ and $H_2{}^{18}O$," J. Quant. Spectrosc. Radiat. Transfer **110**, 573–596 (2009).

[18]T. Furtenbacher, R. Tóbiás, J. Tennyson, O. L. Polyansky, A. A. Kyuberis, R. I. Ovsyannikov, N. F. Zobov, and A. G. Császár, "The W2020 database of validated rovibrational experimental transitions and empirical energy levels of water isotopologues. II. $H_2{}^{17}O$ and $H_2{}^{18}O$ with an update to $H_2{}^{16}O$," J. Phys. Chem. Ref. Data **49**, 043103 (2020).

[19]L. H. Coudert, "Analysis of the rotational levels of water and determination of the potential energy function for the bending ν_2 mode," J. Mol. Spectrosc. **165**, 406–425 (1994).

[20]L. H. Coudert, "Analysis of the line positions and line intensities in the ν_2 band of the water molecule," J. Mol. Spectrosc. **181**, 246–273 (1997).

[21]R. Lanquetin, L. H. Coudert, and C. Camy-Peyret, "High-lying rotational levels of water: Comparison of calculated and experimental energy levels for (000) and (010) up to $J = 25$ and 21," J. Mol. Spectrosc. **195**, 54–67 (1999).

[22]R. Lanquetin, L. H. Coudert, and C. Camy-Peyret, "High-lying rotational levels of water: An analysis of the energy levels of the five first vibrational states," J. Mol. Spectrosc. **206**, 83–103 (2001).

[23]L. H. Coudert, O. Pirali, M. Vervloet, R. Lanquetin, and C. Camy-Peyret, "The eight first vibrational states of the water molecule: measurements and analysis," J. Mol. Spectrosc. **228**, 471–498 (2004).

[24]L. H. Coudert, M.-A. Martin-Drumel, and O. Pirali, "Analysis of the high-resolution water spectrum up to the second triad and to $J = 30$," J. Mol. Spectrosc. **303**, 36–42 (2014).

[25]A. Gambetta, E. Fasci, A. Castrillo, M. Marangoni, G. Galzerano, G. Casa, P. Laporta, and L. Gianfrani, "Frequency metrology in the near-infrared spectrum of $H_2{}^{17}O$ and $H_2{}^{18}O$ molecules: testing a new inversion method for retrieval of energy levels," New J. Phys. **12**, 103006 (2010).

[26]F. C. De Lucia, P. Helminger, R. L. Cook, and W. Gordy, "Submillimeter microwave spectrum of $H_2{}^{18}O$," Phys. Rev. A **6**, 1324–1326 (1972).

[27]S. Belov, I. Kozin, O. Polyansky, M. Tretyakov, and N. Zobov, "Measurement and analysis of precision data on the vibrational and vibrational-rotational spectra of a molecule. the ground and 010 states of $H_2{}^{18}O$," Optics and Spectroscopy **62**, 735–738 (1987).

[28]G. Y. Golubiatnikov, V. N. Markov, A. Guarnieri, and R. Knöchel, "Hyperfine structure of $H_2{}^{16}O$ and $H_2{}^{18}O$ measured by lamb-dip technique in the 180–560 GHz frequency range," J. Mol. Spectrosc. **240**, 251–254 (2006).

[29]F. Matsushima, H. Nagase, T. Nakauchi, H. Odashima, and K. Takagi, "Frequency measurement of pure rotational transitions of $H_2{}^{17}O$ and $H_2{}^{18}O$ from 0.5 to 5 THz," J. Mol. Spectrosc. **193**, 217–223 (1999).

[30]M. L. Diouf, R. Tóbiás, I. Simkó, F. M. J. Cozijn, E. J. Salumbides, W. Ubachs, and A. G. Császár, "Network-based design of near-infrared lamb-dip experiments and the determination of pure rotational energies of $H_2{}^{18}O$ at kHz accuracy," J. Phys. Chem. Ref. Data **50**, 023106 (2021).

[31]E. K. Conway, I. E. Gordon, A. A. Kyuberis, O. L. Polyansky, J. Tennyson, and N. F. Zobov, "Calculated line lists for $H_2{}^{16}O$ and $H_2{}^{18}O$ with extensive comparisons to theoretical and experimental sources including the HITRAN2016 database," J. Quant. Spectrosc. Radiat. Transfer **241**, 106711 (2020).

[32]M. Birk, M. Winnewisser, and E. A. Cohen, "The rotational-torsional spectrum of carbodiimide: A probe for the unusual dynamics," J. Mol. Spectrosc. **136**, 402–445 (1989).

[33]G. Mellau, S. N. Mikhailenko, E. N. Starikova, S. A. Tashkun, H. Over, and V. G. Tyuterev, "Rotational levels of the (000) and (010) states of $D_2{}^{16}O$ from hot emission spectra in the 320–860 cm^{-1} region," J. Mol. Spectrosc. **224**, 32–60 (2004).

[34]S. N. Mikhailenko, G. C. Mellau, E. N. Starikova, S. A. Tashkun, and V. G. Tyuterev, "Analysis of the first triad of interacting states (020), (100), and (001) of $D_2{}^{16}O$ from hot emission spectra," J. Mol. Spectrosc. **233**, 32–59 (2005).

[35]E. N. Starikova, S. N. Mikhailenko, G. C. Mellau, and V. G. Tyuterev, "Analysis of (030),(110), and (011) interacting states of $D_2{}^{16}O$ from hot temperature emission spectra," in *15th Symposium on High-Resolution Molecular Spectroscopy*, Vol. 6580, edited by Y. N. Ponomarev, S. N. Mikhailenko, and L. N. Sinitsa, International Society for Optics and Photonics (SPIE, 2006) p. 658008.

[36]G. C. Mellau, S. N. Mikhailenko, and V. G. Tyuterev, "Hot water emission spectra: Rotational energy levels of the (000) and (010) states of $HD^{17}O$," J. Mol. Spectrosc. **308–309**, 6–19 (2015).

[37]G. C. Mellau, B. P. Winnewisser, and M. Winnewisser, "Near infrared emission spectrum of HCN," J. Mol. Spectrosc. **249**, 23–42 (2008).
[38]S. N. Mikhailenko, V. G. Tyuterev, and G. Mellau, "(000) and (010) States of $H_2{}^{18}O$: analysis of rotational transitions in hot emission spectrum in the 400–850 cm^{-1} region," J. Mol. Spectrosc. **217**, 195–211 (2003).
[39]G. C. Mellau, "SpectrumFit: Analytical spectrum analysis software," (The 18^{th} International Conference on High-Resolution Spectroscopy, Prague, Czech Republic, 2004).
[40]S. N. Mikhailenko, Y. L. Babikov, and V. F. Golovko, "Information-calculating system spectroscopy of atmospheric gases. the structure and main functions," Atmos. and Oceanic Optics **18**, 685–695 (2005).
[41]Spectroscopy of Atmospheric Gases, "Spectra web interface," https://spectra.iao.ru/molecules/simlaunch?mol=1 (2005).
[42]Institute of Atmospheric Optics, Siberian Branch, Russian Academy of Science, Tomsk.
[43]D. W. Schwenke and H. Partridge, "Convergence testing of the analytic representation of an ab initio dipole moment function for water: Improved fitting yields improved intensities," J. Chem. Phys. **113**, 6592–6597 (2000).
[44]S. N. Mikhailenko, S. Béguier, T. A. Odintsova, M. Y. Tretyakov, O. Pirali, and A. Campargue, "The far-infrared spectrum of ^{18}O enriched water vapour (40–700 cm^{-1})," J. Quant. Spectrosc. Radiat. Transfer **253**, 107105 (2020).
[45]L. H. Coudert, G. Wagner, M. Birk, Y. I. Baranov, W. J. Lafferty, and J.-M. Flaud, "The $H_2{}^{16}O$ molecule: Line position and line intensity analyses up to the second triad," J. Mol. Spectrosc. **251**, 339–357 (2008).
[46]S. Yu, J. C. Pearson, B. J. Drouin, M.-A. Martin-Drumel, O. Pirali, M. Vervloet, L. H. Coudert, H. S. P. Müller, and S. Brünken, "Measurement and analysis of new terahertz and far-infrared spectra of high temperature water," J. Mol. Spectrosc. **279**, 16–25 (2012).
[47]L. H. Coudert and P. Chélin, "Line position and line intensity analyses of the high-resolution spectrum of $H_2{}^{18}O$ up to the first triad and $J = 17$," J. Mol. Spectrosc. **326**, 130–135 (2016).
[48]M. Toureille, A. O. Koroleva, S. N. Mikhailenko, O. Pirali, and A. Campargue, "Water vapor absorption spectroscopy and validation tests of databases in the far-infrared (50–720 cm^{-1}). part 1: Natural water," J. Quant. Spectrosc. Radiat. Transfer **291**, 108326 (2022).
[49]R. Radau, "Sur une transformation des équations différentielles de la dynamique," Ann. Sci. Ecole Normale Supérieure **5**, 311–375 (1868).
[50]B. R. Johnson and W. P. Reinhardt, "Adiabatic separations of stretching and bending vibrations: Application to H_2O," J. Chem. Phys. **85**, 4538–4556 (1986).
[51]J. M. Flaud and C. Camy-Peyret, "Vibration-rotation intensities in H_2O-type molecules application to the $2\nu_2$, ν_1, and ν_3 bands of $H_2{}^{16}O$," J. Mol. Spectrosc. **55**, 278–310 (1975).
[52]C. Camy-Peyret and J.-M. Flaud, "Line positions and intensities in the ν_2 band of $H_2{}^{16}O$," Mol. Phys. **32**, 523–537 (1976).
[53]L. H. Coudert, "Line frequency and line intensity analyses of water vapor," Mol. Phys. **96**, 941–954 (1999).
[54]A.-W. Liu, J.-H. Du, K.-F. Song, L. Wang, L. Wan, and S.-M. Hu, "High-resolution Fourier-transform spectroscopy of ^{18}O-enriched water molecule in the 1080–7800 cm^{-1} region," J. Mol. Spectrosc. **237**, 149–162 (2006).
[55]J. W. C. Johns, "High-resolution far-infrared (20–350-cm^{-1}) spectra of several isotopic species of H_2O," J. Opt. Soc. Am. B **2**, 1340–1354 (1985).
[56]C. Oudot, L. Régalia, S. Mikhailenko, X. Thomas, P. V. D. Heyden, and D. Décatoire, "Fourier transform measurements of $H_2{}^{18}O$ and $HD^{18}O$ in the spectral range 1000-2300 cm^{-1}," J. Quant. Spectrosc. Radiat. Transfer **113**, 859–869 (2012).
[57]R. A. Toth, "$2\nu_2 - \nu_2$ and $2\nu_2$ bands of $H_2{}^{16}O$, $H_2{}^{17}O$, and $H_2{}^{18}O$: line positions and strengths," J. Opt. Soc. Am. B **10**, 1526–1544 (1993).
[58]R. A. Toth, "The ν_1 and ν_3 Bands of $H_2{}^{17}O$ and $H_2{}^{18}O$: Line Positions and Strengths," J. Mol. Spectrosc. **166**, 184–203 (1994).
[59]J. Loos, M. Birk, and G. Wagner, "Measurement of positions, intensities and self-broadening line shape parameters of H_2O lines in the spectral ranges 1850–2280 cm^{-1} and 2390–4000 cm^{-1}," J. Quant. Spectrosc. Radiat. Transfer **203**, 119–132 (2017).
[60]F. X. Powell and D. R. Johnson, "Microwave detection of $H_2{}^{18}O$," Phys. Rev. Lett. **24**, 637–637 (1970).
[61]G. Steenbeckeliers and J. Bellet, "Spectre micro-onde des molécules $H_2{}^{16}O$, $H_2{}^{17}O$ et $H_2{}^{18}O$," C. R. Acad. Sci. B **273**, 471–474 (1971).
[62]F. Winther, "The rotational spectrum of water between 650 and 50 cm^{-1}: $H_2{}^{18}O$ and $H_2{}^{17}O$ in natural abundance," J. Mol. Spectrosc. **65**, 405–419 (1977).
[63]R. A. Toth, "Water vapor measurements between 590 and 2582 cm^{-1}: Line postions and strengths," J. Mol. Spectrosc. **190**, 379–396 (1998).
[64]I. Gordon, L. Rothman, R. Hargreaves, R. Hashemi, E. Karlovets, F. Skinner, E. Conway, C. Hill, R. Kochanov, Y. Tan, P. Wciso, A. Finenko, K. Nelson, P. Bernath, M. Birk, V. Boudon, A. Campargue, K. Chance, A. Coustenis, B. Drouin, J. Flaud, R. Gamache, J. Hodges, D. Jacquemart, E. Mlawer, A. Nikitin, V. Perevalov, M. Rotger, J. Tennyson, G. Toon, H. Tran, V. Tyuterev, E. Adkins, A. Baker, A. Barbe, E. Canè, A. Császár, A. Dudaryonok, O. Egorov, A. Fleisher, H. Fleurbaey, A. Foltynowicz, T. Furtenbacher, J. Harrison, J. Hartmann, V. Horneman, X. Huang, T. Karman, J. Karns, S. Kassi, I. Kleiner, V. Kofman, F. KwabiaTchana, N. Lavrentieva, T. Lee, D. Long, A. Lukashevskaya, O. Lyulin, V. Makhnev, W. Matt, S. Massie, M. Melosso, S. Mikhailenko, D. Mondelain, H. Müller, O. Naumenko, A. Perrin, O. Polyansky, E. Raddaoui, P. Raston, Z. Reed, M. Rey, C. Richard, R. Tbis, I. Sadiek, D. Schwenke, E. Starikova, K. Sung, F. Tamassia, S. Tashkun, J. Vander Auwera, I. Vasilenko, A. Vigasin, G. Villanueva, B. Vispoel, G. Wagner, A. Yachmenev, and S. Yurchenko, "The HITRAN2020 molecular spectroscopic database," J. Quant. Spectrosc. Radiat. Transfer **277**, 107949 (2022).